

Internal Report
DESY M 07-01
September 2007

Investigation of the PETRA III Resistive Wall Impedance

M. Ivanyan , E. Laziev, V. Tsakanov, A. Vardanyan
CANDLE, Yerevan, Armenia
A. Tsakanian
Hamburg University, Hamburg, Germany
R. Wanzenberg
DESY, Hamburg, Germany

Deutsches Elektronen-Synchrotron DESY, Hamburg

Investigation of the PETRA III Resistive Wall Impedance

Intermediate Report of the
PETRA III – CANDLE COLLABORATION

M. Ivanyan, E. Laziev, V. Tsakanov, A. Vardanyan

CANDLE, Yerevan, Armenia

A. Tsakanian

Hamburg University, Hamburg, Germany

R. Wanzenberg

DESY, Hamburg, Germany

Abstract

The Report presents the results of the theoretical investigations for the resistive wall impedance of a laminated round tube and its applications to the PETRA III vacuum chambers as well. The general formulae for the impedances of a laminated round vacuum chamber with an arbitrary number of layers are given. The results for an arbitrary Lorentz-factor and in the ultra-relativistic limit are presented. An analysis of the longitudinal and transverse impedance of the e PETRA III vacuum chambers has been performed. The kick factor and the integrated gradient of the longitudinal wake potential have been calculated for the PETRA III vacuum chambers taking into account the finite thickness of the chamber wall and the coating of the wall with NEG material. The dependence of those parameters on the thickness of the wall and the NEG coating have been investigated, too. The results have been compared with the long range approximation of the resistive wall and the domain of validity for this approximation has been investigated as well. The contribution of longitudinal and transverse resistive wall impedances of the vacuum chambers to the total impedance budget of PETRA III was determined.

CONTENTS

1. Introduction.....	3
2. Resistive wall impedance for multilayer round tube.....	5
3. Ultra-relativistic limit.....	10
4. Numerical investigations.....	12
4.1. Longitudinal and transverse impedances - modal expansion terms	12
4.2. Longitudinal and transverse impedances - presentation of the modal expansion terms. Low-frequency region.....	13
4.3. NEG coating.....	15
4.4. Frequency-dependent conductivity.....	15
4.5. Transverse loss factor (kick factor).....	16
4.6. Total kick parameter for resistive walls.....	21
4.7. Integral gradient of the longitudinal wake.....	22
4.8. PETRA III resistive impedance budget.....	24
5. Conclusion.....	25
6. Acknowledgment.....	25
7. References.....	25

1. Introduction

The present intermediate report includes the investigations performed within the framework of the PETRAIII-CANDLE Collaboration. CANDLE is participating in the study of the impedances and wakefields of the PETRA III synchrotron light source. The CANDLE participates in the following Tasks:

1. The longitudinal and transverse AC and DC resistive wall impedance of a standard vacuum chamber of the ring with circular and elliptical cross sections.
2. The longitudinal and transverse impedances of the elliptical vacuum chamber of the undulator and wiggler sections, including the aluminum vacuum chamber, which is coated with NEG material. The results should be compared with the published results of the measurements from existing synchrotron light sources.
3. The study of the vacuum chamber heating due to resistive wake fields.
4. The impedances due to the metal coating of the ceramic vacuum chamber of the injection kicker.

The geometry and wall material of vacuum chambers, which are considered in the report, are presented in Table 1 [1].

N	Denomination	Material	Form	Inner dimensions	Coating material	Coating thickness	Wall thickness
1	Standard arc	Aluminum	Elliptical	$r_1=40\text{mm}$, $r_2=20\text{mm}$	-	-	4mm
2	Standard straight section	Stainless Steel	Circular	$R=47\text{mm}$	-	-	2mm
3	Undulator vacuum chamber	Aluminum	Elliptical	$r_1=28.5\text{mm}$, $r_2=3.5\text{mm}$	-	-	1mm
4	Wiggler vacuum chamber	Aluminum	Elliptical	$r_1=48\text{mm}$, $r_2=8.95\text{mm}$	NEG	0.5-1 μm	2.8mm

Table 1: Main parameters of the PETRA III vacuum chambers.

Electrical conductivities of the used materials are given in Table 2, [1].

Material	Conductivity ($\Omega\text{m})^{-1}$
Copper	$58.0 \cdot 10^6$
Aluminum	$36.6 \cdot 10^6$
Stainless Steel	$1.5 \cdot 10^6$
NEG (Ti V Zr)	$0.31 \cdot 10^6$

Table 2: Electrical conductivity of wall material.

In Table 3 the main machine parameters of PETRA III are summarized [2].

Energy	6 GeV
RMS bunch length	12 mm
Emittance	1 nm rad
Coupling ($\varepsilon_y/\varepsilon_x$)	1 %
Total current	100 mA
Total number of buckets	3840
Number of bunches	40 and 960
Beam lifetime (100 mA)	2 h and 24 h
Run lifetime	Top-up
Drifts for 5m-undulators	3
Drifts for 2m-undulators	10
Drifts for 20m-undulators	1
Sections for wigglers (2 x 10 x 4 m)	West and Nord

Table 3: Main parameters of PETRA III.

In the framework of the PETRA III - CANDLE collaboration the following investigations have been done:

1. The wake fields due to a point-like charge passing through a circular tube with multi-layer walls with an arbitrary number of layers have been calculated. The thickness of the wall is finite. In our model arbitrary properties of the material (including magnetic ones) can be used for the filling of the layers. The charge moves with an arbitrary constant velocity parallel to the tube axis. The problem is solved with the field-matching method for an arbitrary field harmonic. Exact solutions and ultra-relativistic limits for the field harmonic, in the inner part of tube and for the external fields as well, have been obtained.

2. A program based on the Mathematica 5 software package has been created to calculate the longitudinal and transverse impedance for an arbitrary number of layers and gamma factor (including the ultra-relativistic limit) .
3. Numerical calculations of the longitudinal and transverse resistive wall impedances of the PETRA III vacuum chambers have been performed. The integral parameters: gradient of the longitudinal wake potential and transverse kick factor have been calculated as well. The resistive wall impedance budget for the PETRA III devices was composed.

2. Resistive wall impedance for multilayer round tube

A round tube is often used as a working model of vacuum chambers and other elements of the accelerating structures. Some components of accelerating facilities have a round form in reality (see, for example, [1]), but even in the case of more complicated cross sections the round tube approximation permits one to do the qualitative estimation of impedances of these structures. The classical ultra-relativistic formulae [3,4], generally used for the impedance calculation, were derived for the homogeneous unbounded single-layer tube [3] and generalized for the case of one finite-width metallic [3] or ceramic [5] internal cover. The methods based on the numerical rigorous solutions of the boundary conditions equations, using recursive expressions for the arbitrary number of layers, are given in [5-8]. An analytical solution for a single layer tube with a finite thickness of the wall was obtained in [9], and an expression for the transverse dipole impedance of a two-layer tube (with an externally unbounded outside layer) was derived in [8]. An increasing number of layers leads to a growing number of the boundary equations, which involves difficulties especially in the process of finding an analytical solution. Some analytical and numerical studies of the impedance for multi-layer tube are given in several references [10-17]. A simple exact formula for the monopole impedance of the two-layer tube with a finite wall thickness in the ultra-relativistic limit has been derived in [18]. For the same geometry more complicated formulae, but which can still be used for direct numerical calculations, are given in [19] for the multipole components of the impedance. The case of a three-layer tube is already difficult to solve [20], caused by the complications of modelling and calculations [21].

The plain disk-like charge was taken as a basic model for the driving charge in references [3-7, 18, 19]. In the ultra-relativistic limit the model allows an interpretation of the results as the multipole expansion of the impedance of a point-like charge [19, 22], but for a non-relativistic beam the fields pattern, generated by a disk-like charge, differs essentially from the point-like one. In this report we are using the basic definition of the impedance [3] with a point-like charge as a driving source. We are presenting the field of a driving point-like charge in terms of field harmonics [23]

and we have derived the internal and external exiting field components for an arbitrary velocity of the charge and for a multi-layer tube with finite wall thickness and an arbitrary number of layers. The ultra-relativistic limit of the solution is obtained as well. The results have been compared with the existing ones [3-5, 9, 18], and the uniform convergence of the exact solution to the ultra-relativistic approximation has been shown as well.

For an arbitrary γ (relativistic factor), and a homogeneous infinite tube (with arbitrary cross-section) the longitudinal and transverse coupling impedances per unit length may be expressed as a Fourier transformation of the longitudinal or transverse normalized component of the Lorentz force, which is independent from the longitudinal coordinate (z) [5]:

$$Z_{\parallel}(\omega, \gamma, \vec{r}, \vec{r}_s) = -\frac{E_z^o(\omega, \gamma, \vec{r}, \vec{r}_s)}{e}, \quad (2.1)$$

$$\vec{Z}_{\perp}(\omega, \gamma, \vec{r}, \vec{r}_s) = -\frac{j}{e} \left(\vec{E}_{\perp}^o(\omega, \gamma, \vec{r}, \vec{r}_s) - [\vec{v} \times \vec{B}^o(\omega, \gamma, \vec{r}, \vec{r}_s)]_{\perp} \right), \quad (2.2)$$

where e and $v = v_z$ are the value and velocity of the driving charge, traversing the tube parallel to the longitudinal axis; ω is the revolution frequency, \vec{r}_s, \vec{r} are the positions of the driving and test charge; \vec{E}^o and \vec{B}^o are the electric field strength and the magnetic induction respectively, produced by the charge. Both, the longitudinal and the transverse impedance may be presented as a sum of two terms in the general case of a wall with a finite conductivity:

$$Z_{\parallel} = Z_{\parallel}^R + Z_{\parallel}^{\infty}, \quad \vec{Z}_{\perp} = \vec{Z}_{\perp}^R + \vec{Z}_{\perp}^{\infty}, \quad (2.3)$$

where the second term describes the impedance of an ideal conducting wall and the first one presents the impact of the finite conductivity of the wall, and can be interpreted as the resistive wall impedance.

As it was mentioned above, for the adequate presentation of the impedance it is necessary to take into account the finite thickness of the vacuum chamber wall and its lamination.

We are examining the homogeneous infinite multi-layer round tube with finite wall thickness and with vacuum in its inner and outer sides (Fig.1). The outer and inner radii of the tube are equal to a_0 and a_m (m the layer's number) correspondingly. Each layer is filled with a material with an arbitrary dielectrical permittivity ε_i and magnetic permeability μ_i ($i = 1, 2, 3, \dots, m$). The point-like charge is moving with the constant velocity v (less than speed of light c) parallel to the axis of the tube with an offset r_s .

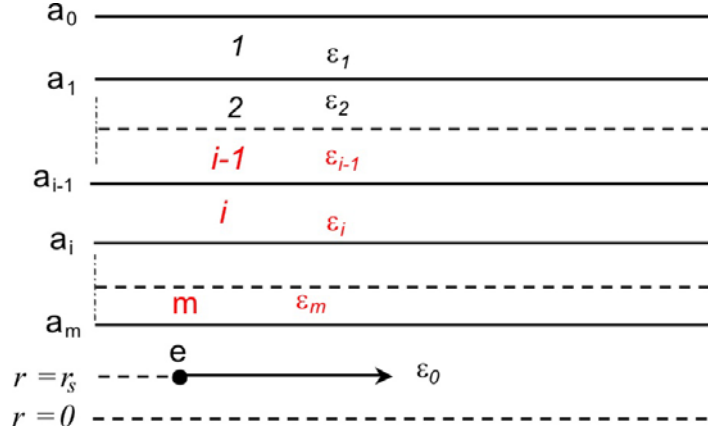


Fig.1: Point-like charge in a multi-layer tube with a finite wall thickness.

The modal expansion terms of the resistive wall longitudinal coupling impedance for the round multiplayer tube with an arbitrary number of layers, based on the exact solution of the Maxwell equations, are presented below:

$$Z_{\parallel}^{(n)} = -\frac{E_z^o}{e} = -\frac{1}{e} \tau I_n(\lambda r) D_2 \cos(n\varphi) - \frac{E_z^\infty}{e} \cos(n\varphi). \quad (2.4)$$

For the same case, the harmonic components of the transverse impedance can be presented in the following way:

$$\begin{aligned} Z_{\perp r}^{(n)} &= -\frac{j}{e} (E_r^o - v B_\varphi^o) = -\frac{1}{e} \tau^2 D_2 I_n'(\lambda r) \cos(n\varphi) - j \frac{E_r^\infty}{e} \tau^2 \cos(n\varphi), \\ Z_{\perp \varphi}^{(n)} &= -\frac{j}{e} (E_\varphi^o + v B_r^o) = \frac{1}{e} \tau D_2 n \frac{I_n(\lambda r)}{k_v r} \sin(n\varphi) - j E_\varphi^\infty \tau^2 \sin(n\varphi), \end{aligned} \quad (2.5)$$

where D_2 is a constant coefficient, $I_n(x)$ is a modified Bessel function of the first kind ($n=0,1,2,\dots$), $\lambda = k_v \tau$, $k_v = \omega/v$ and $\tau = \gamma^{-1}$. The second term in (2.4), (2.5) presents the contribution the impedance from ideal conducting wall:

$$\begin{aligned} E_\varphi^\infty &= -v B_r^\infty / \beta^2 = -\frac{j n U^o I_n(\lambda r_<)}{\lambda r I_n(\lambda a_m)} (I_n(\lambda r_>) K_n(\lambda a_m) - K_n(\lambda r_>) I_n(\lambda a_m)), \\ E_z^\infty &= -\frac{U^o \tau I_n(\lambda r_<)}{I_n(\lambda a_m)} (I_n(\lambda r_>) K_n(\lambda a_m) - K_n(\lambda r_>) I_n(\lambda a_m)), \quad j v B_z^\infty = 0, \\ E_r^\infty &= v B_\varphi^\infty / \beta^2 = \frac{j U^o \xi_n(\lambda r_<)}{I_n(\lambda a_m)} (\xi_n(\lambda r_>) K_n(\lambda a_m) - \eta_n(\lambda r_>) I_n(\lambda a_m)), \end{aligned} \quad (2.6)$$

where $0 \leq r \leq a_m$ (a_m is the inner radius of the tube),

$$\begin{aligned}
U^o &= -j \frac{e}{2\pi} \frac{\lambda}{\varepsilon_0 v} (2 - \delta_{0,n}), \\
\xi_n(\lambda x) &= \begin{cases} I'_n(\lambda r), & \text{if } x = r \\ I_n(\lambda r_s), & \text{if } x = r_s \end{cases}, \quad \eta_n(\lambda x) = \begin{cases} K'_n(\lambda r), & \text{if } x = r \\ K_n(\lambda r_s), & \text{if } x = r_s \end{cases}, \\
r_{>} &= \begin{cases} r & \text{if } r \geq r_s \\ r_s & \text{if } r \leq r_s \end{cases}, \quad r_{<} = \begin{cases} r_s & \text{if } r \geq r_s \\ r & \text{if } r \leq r_s \end{cases}
\end{aligned} \tag{2.7}$$

with $\delta_{0,0} = 1$, $\delta_{0,n>0} = 0$ and $K_n(x)$ is the modified Bessel function of the second kind ($n = 0, 1, 2, \dots$); The external field components ($a_0 \leq r < \infty$, where $a_0 > a_m$ is the external radius of the tube) may be presented in the following way:

$$\begin{aligned}
E_z^r(\lambda r) &= \tau D_4 K_n(\lambda r), \quad jvB_z^r(\lambda r) = -\tau D_3 K_n(\lambda r) \\
\left. \begin{matrix} E_\phi^r \\ E_r^r \end{matrix} \right\} &= \{ (D_3 + jD_4)K_{n+1}(\lambda r) \pm (D_3 - jD_4)K_{n-1}(\lambda r) \} / 2 \\
\left. \begin{matrix} vB_\phi^r \\ vB_r^r \end{matrix} \right\} &= \{ \pm (D_3 + j\beta^2 D_4)K_{n+1}(\lambda r) - (D_3 - j\beta^2 D_4)K_{n-1}(\lambda r) \} / 2
\end{aligned} \tag{2.8}$$

The coefficient D_2 in (2.5) for the impedance and the coefficients D_3 and D_4 (2.8) for the external radiation are being determined by the following formulae (the coefficient D_1 is used in the expression for the internal field, which is not presented here):

$$D_i = -jvB_\phi^\infty G_i / G, \quad i = 1, 2, 3, 4 \tag{2.9}$$

with $vB_\phi^\infty = \frac{e}{2\pi} \frac{Z_0}{a_m} (2 - \delta_{0,n}) \beta \frac{I_n(\lambda r_s)}{I_n(\lambda a_m)}$, $Z_0 = 120\pi \Omega$ the impedance of free space, and

$$\begin{aligned}
G_1 &= \frac{jnI_n(\xi_m)}{\xi_m} F_{42} - \tau I_n(\xi_m) F_{41}, \\
G_2 &= I'_n(\xi_m) F_{42} + \tau I_n(\xi_m) F_{21}, \\
G_3 &= -\tau I_n(\xi_m) \left(\mathcal{I}_n(\xi_m) \Pi_1 - jn \frac{I_n(\xi_m)}{\xi_m} \Pi_2 - I'_n(\xi_m) \Pi_4 \right) \\
G_4 &= -\tau I_n(\xi_m) \left(\mathcal{I}'_n(\xi_m) \Pi'_1 - jn \frac{I_n(\xi_m)}{\xi_m} \Pi'_2 - I'_n(\xi_m) \Pi'_4 \right) \\
G &= \frac{jnI_n(\xi_m)}{\xi_m} G_1 + \beta^2 I'_n(\xi_m) G_2 + \mathcal{I}_n(\xi_m) (\Pi'_3 \tilde{G}_3 - \Pi_3 \tilde{G}_4)
\end{aligned} \tag{2.10}$$

where

$$\begin{aligned}
\Pi_s &= \frac{jnK_n(\xi_0)}{\xi_0} H_{s,1} + \beta^2 H_{s,3} K_n'(\xi_0) + H_{s,2} \tau K_n(\xi_0) \\
\Pi_s' &= -\frac{jnK_n(\xi_0)}{\xi_0} H_{s,3} + H_{s,1} K_n'(\xi_0) + H_{s,4} \tau K_n(\xi_0) \\
F_{ij} &= -\Pi_i \Pi_j' + \Pi_j \Pi_i'
\end{aligned} \tag{2.11}$$

with $\xi_0 = k_v a_0 \tau$ and $\xi_m = k_v a_m \tau$. The coefficients $H_{s,j}$, ($s, j = 1, 2, 3, 4$) are the elements of a 4×4 matrix, which is a product of m (m is a number of layers) matrixes:

$$\widehat{H}^{(m)} = \widehat{Q}^{(m)} \widehat{Q}^{(m-1)} \dots \widehat{Q}^{(2)} \widehat{Q}^{(1)} \tag{2.12}$$

The matrix $\widehat{Q}^{(i)}$, ($i = 1, 2, \dots, m$) is also a 4×4 matrix, in which the electrical properties of the material of the i -th layer and its geometrical dimensions are included:

$$\widehat{Q}^{(i)} = \begin{pmatrix} q_{11} & q_{12} & -\alpha_i q_{31} & \alpha_i q_{32} \\ 0 & q_{22} & \alpha_i q_{41} & -\alpha_i q_{42} \\ q_{31} & q_{32} & q_{11} & -q_{12} \\ q_{41} & q_{42} & 0 & q_{22} \end{pmatrix} \tag{2.13}$$

where

$$\alpha_i = \frac{\mu_i \varepsilon_0}{\mu_0 \varepsilon_i} \frac{1}{\beta^2} \tag{2.14}$$

and

$$\begin{aligned}
q_{11} &= -a_{i-1} \chi_i U_3^{(i)}, & q_{12} &= j \frac{k_v n}{a_i \chi_i} (a_{i-1} U_2^{(i)} + a_i U_3^{(i)}), & q_{22} &= a_{i-1} \chi_i U_2^{(i)}, \\
q_{31} &= j \frac{\mu_0}{\mu_i} \frac{a_{i-1}}{a_i} n U_1^{(i)}, & q_{32} &= k_v \left(\beta^2 \frac{\varepsilon_i}{\varepsilon_0} a_{i-1} U_4^{(i)} + \frac{\mu_0}{\mu_i} \frac{n^2 U_1^{(i)}}{a_i \chi_i^2} \right), & & \\
q_{41} &= -\frac{a_{i-1} \mu_0 \chi_i^2}{k_v \mu_i} U_1^{(i)}, & q_{42} &= j \frac{\mu_0}{\mu_i} n U_1^{(i)}. & &
\end{aligned} \tag{2.15}$$

In (2.15): a_{i-1} and a_i are the outer and inner radii of the i -th layer with the arbitrary dielectric permittivity ε_i and magnetic permeability μ_i ($i = 1, 2, 3, \dots, m$); $\chi_i^2 = k_v^2 - \omega^2 \varepsilon_i \mu_i$ ($\text{Re } \chi_i > 0$) is a transverse propagation constant. The functions $U_j^{(i)}$ ($i = 1, 2, \dots, m$, $j = 1, 2, 3, 4$) have the following form:

$$U_1^{(i)} = K_n(\chi_i a_i) I_n(\chi_i a_{i-1}) - I_n(\chi_i a_i) K_n(\chi_i a_{i-1}) \approx \text{Sh}(\chi_i d_i) / \chi_i \sqrt{a_{i-1} a_i}$$

$$\begin{aligned}
U_2^{(i)} &= K_n(\chi_i a_i) I_n'(\chi_i a_{i-1}) - I_n(\chi_i a_i) K_n'(\chi_i a_{i-1}) \approx Ch(\chi_i d_i) / \chi_i \sqrt{a_{i-1} a_i} \\
U_3^{(i)} &= K_n'(\chi_i a_i) I_n(\chi_i a_{i-1}) - I_n'(\chi_i a_i) K_n(\chi_i a_{i-1}) \approx -Ch(\chi_i d_i) / \chi_i \sqrt{a_{i-1} a_i} \\
U_4^{(i)} &= K_n'(\chi_i a_i) I_n'(\chi_i a_{i-1}) - I_n'(\chi_i a_i) K_n'(\chi_i a_{i-1}) \approx -Sh(\chi_i d_i) / \chi_i \sqrt{a_{i-1} a_i}
\end{aligned} \tag{2.16}$$

where $d_i = a_{i-1} - a_i$ is the thickness of the i -th layer.

The above functions (2.16) satisfy the following expression:

$$U_1^{(i)} U_4^{(i)} - U_2^{(i)} U_3^{(i)} = (a_{i-1} a_i \chi_i^2)^{-1} \tag{2.17}$$

An approximate presentation of the functions $U_i^{(j)}$, given in (2.16), is often used to construct asymptotic expressions of the impedance [4, 15,16,19] which is valid for all frequencies where the skin depth of the layer is much smaller as the inner radius of the tube, i.e. for all practically important cases.

3. Ultra-relativistic limit

The results, presented in previous Chapter, can be used to investigate the impedances of a multi-layer tube and also the external radiated field for an arbitrary number of layers. The results are valid for an arbitrary value of γ . Furthermore, an ultra-relativistic approximation, which permits an accurate calculation of the impedances and external radiation in the case of large γ (which is appropriate enough for such facilities as PETRA III), is presented below:

For $n = 0$:

$$Z_{\parallel}^{(0)} = j \frac{Z_0}{\pi k_c a_m^2} \left(1 - \frac{2}{k_c a_m} \frac{\widehat{H}_{33}}{\widehat{H}_{23}} \right)^{-1} \tag{3.1}$$

For $n = 1$:

$$\begin{aligned}
Z_{\parallel}^{(1)} &= -j \frac{2Z_0 k_c}{\pi} \frac{V_b'}{V_b'(2 - k_c^2 a_m^2) - 2k_c a_m V_b^{(+)}} \frac{r}{a_m} \frac{r_s}{a_m} \cos \varphi \\
Z_r^{(1)} &= -j \frac{2Z_0}{\pi a_m^2} \frac{V_b'}{V_b'(2 - k_c^2 a_m^2) - 2k_c a_m V_b^{(+)}} r_s \cos \varphi \\
Z_{\varphi}^{(1)} &= j \frac{2Z_0}{\pi a_m^2} \frac{V_b'}{V_b'(2 - k_c^2 a_m^2) - 2k_c a_m V_b^{(+)}} r_s \sin \varphi
\end{aligned} \tag{3.2}$$

For $n > 1$:

$$\begin{aligned}
Z_{\parallel}^{(n)} &= j \frac{Z_0}{\pi} k_c \left(\frac{k_c^2 a_m^2}{n+1} + \frac{k_c a_m Q^{(+)}}{Q'} - n \right)^{-1} \left(\frac{r}{a_m} \right)^n \left(\frac{r_s}{a_m} \right)^n \cos(n\varphi) \\
Z_r^{(n)} &= j \frac{nZ_0}{\pi a_m} \left(\frac{k_c^2 a_m^2}{n+1} + \frac{k_c a_m Q^{(+)}}{Q'} - n \right)^{-1} \left(\frac{r}{a_m} \right)^{n-1} \left(\frac{r_s}{a_m} \right)^n \cos(n\varphi) \\
Z_{\varphi}^{(n)} &= -j \frac{nZ_0}{\pi a_m} \left(\frac{k_c^2 a_m^2}{n+1} + \frac{k_c a_m Q^{(+)}}{Q'} - n \right)^{-1} \left(\frac{r}{a_m} \right)^{n-1} \left(\frac{r_s}{a_m} \right)^n \sin(n\varphi)
\end{aligned} \tag{3.3}$$

The following expressions are used in (3.1)-(3.3):

$$\begin{aligned}
V_b' &= B' + k_c a_0 A' + 2k_c^2 a_0^2 B' V_{a_0}, \\
V_b^{(\pm)} &= B^{(\pm)} + k_c a_0 A^{(\pm)} + 2k_c^2 a_0^2 B^{(\pm)} V_{a_0}, \\
V_{a_0} &= \ln(k_c a_0 \tau / 2) + C_E
\end{aligned} \tag{3.4}$$

with the Euler constant $C_E = 0.577216$, $Z_0 = 120\pi \Omega$ the impedance of free space, and

$$\begin{aligned}
Q^{(\pm)} &= B^{(\pm)} F_0 + (n-1) k_c a_0 A^{(\pm)} \\
Q' &= B' F_0 + (n-1) k_c a_0 A' \\
F_0 &= n(n-1) - k_c^2 a_0^2 \\
A_m^{(\pm)} &= \text{Det} \left[\widehat{h}_{11;22}^{(+)} + \widehat{h}_{33;44}^{(\pm)} + j \left(\widehat{h}_{13;24}^{(+)} - \widehat{h}_{31;42}^{(\pm)} \right) \right], \quad B_m^{(\pm)} = \text{Det} \left[\widehat{h}_{11;23}^{(+)} - j \widehat{h}_{31;43}^{(\pm)} \right] \\
A_m' &= \text{Det} \left[\widehat{h}_{21;42}^{(+)} + j \widehat{h}_{23;44}^{(+)} \right], \quad B_m' = \text{Det} \left[\widehat{h}_{21;43}^{(+)} \right].
\end{aligned} \tag{3.5}$$

The coefficients $A_m^{(\pm)}$, $B_m^{(\pm)}$, A_m' and B_m' (3.5) can be expressed as combinations of the limiting form of the elements of the matrix $\widehat{H}^{(m)}$:

$$\widehat{h}_{pi;qj}^{(\pm)} = \begin{Bmatrix} \pm \widehat{H}_{pi} & \pm \widehat{H}_{pj} \\ \widehat{H}_{qi} & \widehat{H}_{qj} \end{Bmatrix}, \quad \widehat{H}_{sl} = \widehat{H}_{sl} |_{\beta=1} \tag{3.6}$$

Thus, the impedances may be presented as a multipole expansion series:

$$Z_{\parallel} = \sum_{n=0}^{\infty} \widetilde{Z}_{\parallel}^{(n)} \left(\frac{r}{a_m} \right)^n \left(\frac{r_s}{a_m} \right)^n \cos(n\varphi) \tag{3.7}$$

where

$$\tilde{Z}_{\parallel}^{(n)} = \begin{cases} j \frac{Z_0}{\pi k_c a_m^2} \left(1 - \frac{2}{k_c a_m} \frac{\tilde{H}_{33}}{\tilde{H}_{23}} \right)^{-1} & \text{for } n=0 \\ -j \frac{2Z_0 k_c}{\pi} \frac{V'_b}{V'_b (2 - k_c^2 a_m^2) - 2k_c a_m V_b^{(+)}} & \text{for } n=1 \\ j \frac{Z_0}{\pi} k_c \left(\frac{k_c^2 a_m^2}{n+1} + \frac{k_c a_m Q^{(+)}}{Q'} - n \right)^{-1} & \text{for } n > 1 \end{cases} \quad (3.8)$$

$$Z_r = \sum_{n=1}^{\infty} \tilde{Z}_T^{(n)} \left(\frac{r}{a_m} \right)^{n-1} \left(\frac{r_s}{a_m} \right)^n \cos(n\varphi), \quad Z_{\varphi} = -\sum_{n=1}^{\infty} \tilde{Z}_T^{(n)} \left(\frac{r}{a_m} \right)^{n-1} \left(\frac{r_s}{a_m} \right)^n \sin(n\varphi) \quad (3.9)$$

where

$$\tilde{Z}_T^{(n)} = \frac{n \tilde{Z}_{\parallel}^{(n)}}{k_c a_m} \quad (3.10)$$

The above expressions satisfy the Panofsky-Wenzel theorem [5]:

$$\nabla_{\perp} Z_{\parallel}^{(n)} = k_c \vec{Z}_{\perp}^{(n)} \quad (3.11)$$

4. Numerical investigations

Using the results, presented in Chapters 2 and 3, the following impedance calculation for PETRA III has been made:

4.1 Longitudinal and transverse impedances- modal expansion terms.

The following graphics have been made for the PETRA III straight section (see Table 2, No 2).

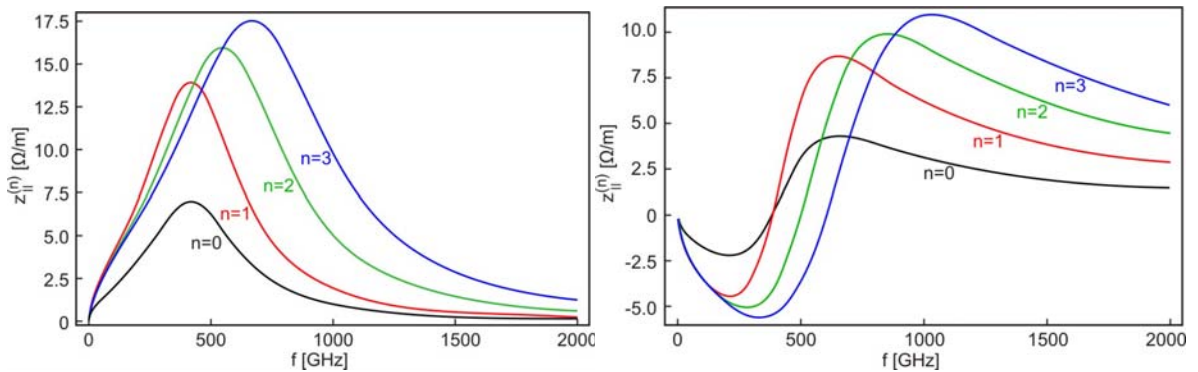


Fig. 2: Real (left) and imaginary (right) parts of longitudinal impedance multipole distribution versus frequency. Tube material: stainless steel, inner radius of the tube: 47mm. The wall thickness is 2mm.

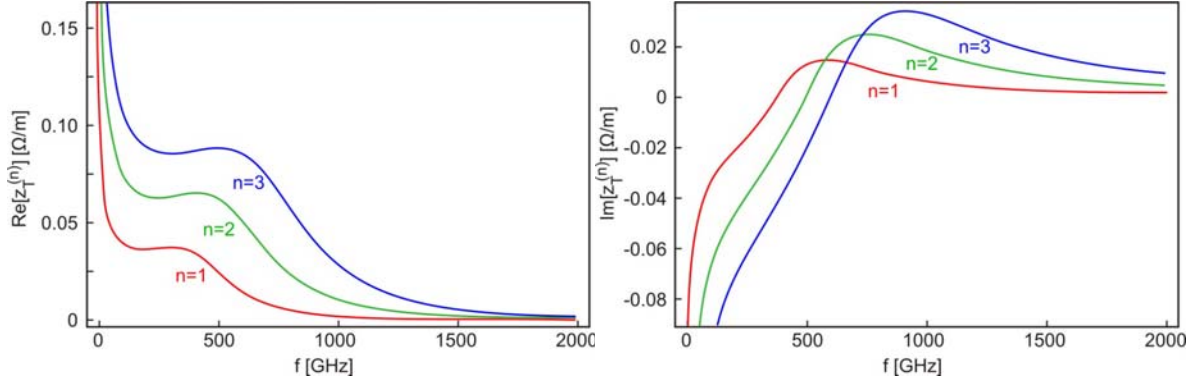


Fig. 3: Real (left) and imaginary (right) parts of transverse impedance multipole distribution versus frequency. Tube material: stainless steel, inner radius of the tube: 47mm. The wall thickness is 2 mm.

The graphs, presented on Fig. 2 and 3, are calculated for the ultra-relativistic limit according to formula (3.8) for the longitudinal impedance and according to formulae (3.10) for the transverse impedance. For a wall thickness of 2 mm the skin depth is equal to the wall thickness when the frequency is equal to $f_0 \sim 42\text{kHz}$. For frequencies $f \gg f_0$ the above results coincide with the results, calculated according to formulae, which are generally used for the impedance estimation and have been obtained for unbounded tube wall [3]:

$$\tilde{Z}_{\parallel}^{(n)} = \begin{cases} \frac{Z_0 \zeta_0}{2\pi b^2} \left(\frac{1+j}{\sqrt{\kappa}} - \frac{j\kappa}{2} \right)^{-1} & \text{for } n=0 \\ \frac{Z_0 \zeta_0}{\pi b^2} \left(\frac{1+j}{\sqrt{\kappa}} - \frac{j\kappa}{(n+1)} \right)^{-1} & \text{for } n>0 \end{cases} \quad (4.1)$$

$$\tilde{Z}_T^{(n)} = n\tilde{Z}_{\parallel}^{(n)}/kb \quad \text{for } n>0$$

where $b = a_m$ is the inner radius of the tube, $\kappa = k\zeta_0$ is a dimensionless wave number, and

$$\zeta_0 = \left(2b^2/Z_0\sigma \right)^{1/3} \quad (4.2)$$

is a characteristic parameter of the tube, with σ the conductivity of the wall material [4].

4.2 Longitudinal and transverse impedances – presentation of the modal expansion terms.

Low-frequency region

The difference arises for the frequencies $f \leq f_0$. Figures 4 and 5 show the real and

imaginary parts of the longitudinal monopole and transverse dipole impedance ($\tilde{Z}_{\parallel}^{(0)}$ and $\tilde{Z}_T^{(1)}$ in (3.8) and (3.10)) in the kHz-frequencies region in comparison with the results, obtained according to formulae (4.1).

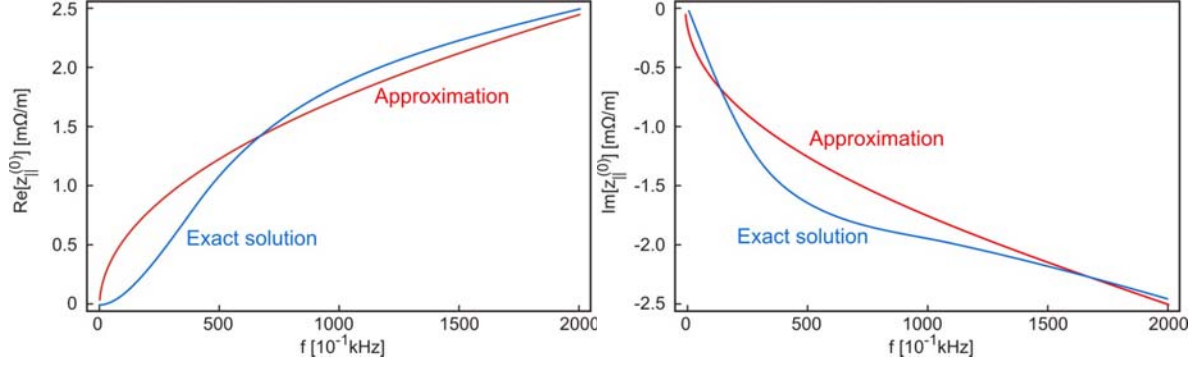


Fig. 4: Real and imaginary parts of longitudinal monopole impedance (Exact solution) in the kHz-frequency region in comparison with the results, obtained according to formula (4.1) (Approximation).

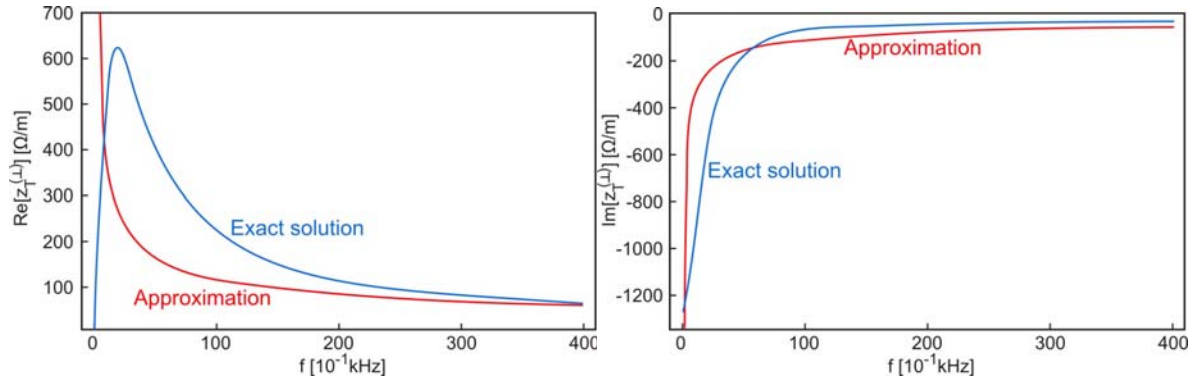


Fig. 5: Real and imaginary parts of the transverse dipole impedance (Exact solution) in the kHz-frequency region in comparison with the results, obtained according to formulae (4.1) (Approximation).

As one can see from Figure 5, the transverse impedance, obtained by general formulae (4.1),(4.2), diverges at $\omega = 0$, while the same one, obtained by the exact formula has a finite value at zero frequency. This value is equal to $Z_T^{(n)}(\omega = 0) = -jZ_0/2\pi b$ and does not depend on material, or thickness of the layers and the multipole number.

4.3 NEG coating

If the inner wall of the tube, which has been investigated in sections 4.1 and 4.2, is coated with NEG material ($\sigma_{NEG} = 0.31 \cdot 10^6 \Omega^{-1} m^{-1}$) with a thickness of $1 \mu m$, the frequency that corresponds to the skin depth equal to cover thickness is in order of $f_0 \sim 820 GHz$. For this case, as it can be seen from Fig. 6, the impact of the NEG-coating is visible for frequencies $f \geq 5 - 10 GHz$.

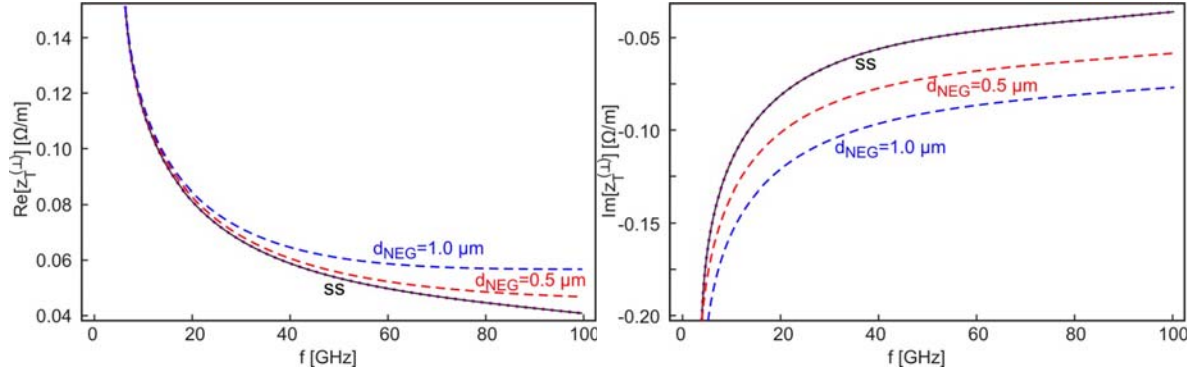


Fig. 6: Real and imaginary parts of the transverse dipole impedance for a stainless steel tube with an inner radius of 47 mm (wall thickness 2 mm) with an inner NEG coating, which is $1 \mu m$ and $0.5 \mu m$ thick. The impedance of a stainless steel (SS) tube without coating is also shown, calculated according to the formulae (3.8) and (3.10) (points) and formula (4.1) (solid curve). The solid curve coincides with the dotted curve.

4.4 Frequency-dependent conductivity

Taking into account the frequency dependence of the conductivity of the metal, the conductivity can be presented as:

$$\sigma(\omega) = \sigma_{st} (1 - j\omega\tau)^{-1} \quad (4.3)$$

where σ_{st} is the static conductivity and τ is a relaxation time. A comparison of the longitudinal impedance of the stainless steel tube with a frequency dependent (AC) and a frequency independent (DC) conductivity is presented in Fig. 7. The relaxation time is taken to be equal to $\tau = 3.2 \cdot 10^{-14}$ sec, which corresponds to the relaxation time of iron at a temperature $T = 77$ K. The transverse dipole impedance for the same tube is presented in Figure 8.

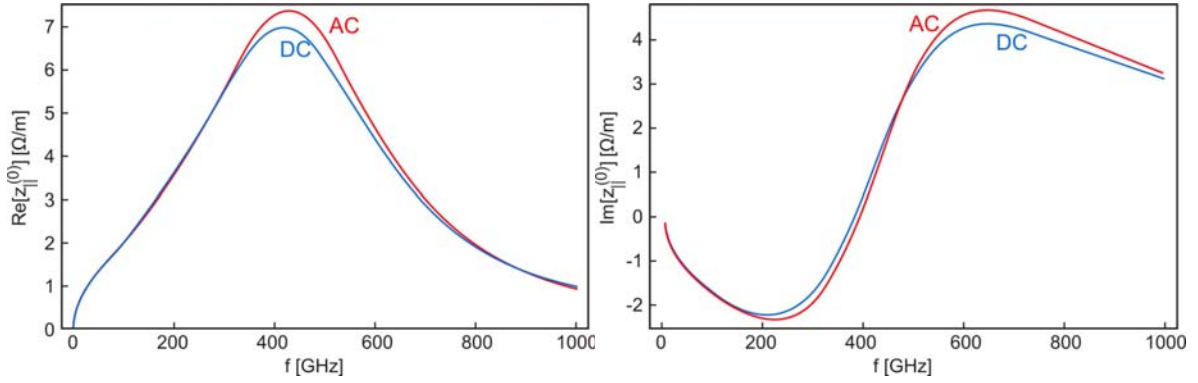


Fig. 7: Longitudinal monopole impedance of a stainless steel tube (inner radius 47 mm, wall thickness 2 mm) for DC and AC conductivities.

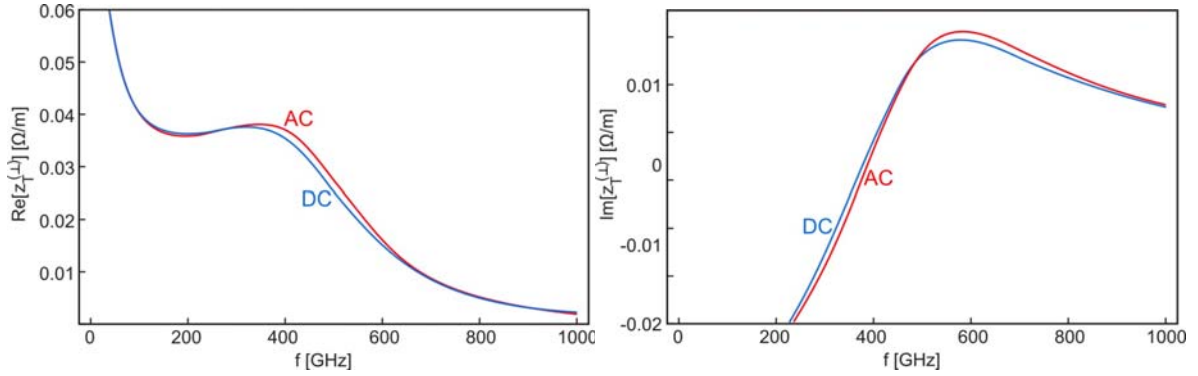


Fig. 8: Transverse dipole impedance of a stainless steel tube (inner radius 47 mm, wall thickness 2 mm) for DC and AC conductivities.

The results, given in Figure 7, may be compared with the similar curves for a longitudinal monopole impedance with an AC conductivity, presented in [4], where the dimensionless parameter $\Gamma = \tau \cdot c / \zeta_0$ is equal to 0.4. In our case (Fig. 7, 8) the same parameter is equal to 0.048. For a copper tube with the same inner radius the value of Γ will be noticeably larger: $\Gamma = 1.07$ at $T = 77K$ and $\Gamma = 0.14$ for $T = 273K$.

4.5 Transverse loss factor (kick factor)

The transverse loss factor for a beam with a RMS longitudinal size σ can be determined as an integral in frequency domain in the following way [5]:

$$\kappa_T(\sigma) = \frac{1}{2\pi} \int_{-\infty}^{\infty} dz Z_T(\omega) h(\omega, \sigma) = \frac{1}{\pi} \int_0^{\infty} dz \text{Im}[Z_T(\omega)] h(\omega, \sigma) \quad (4.4)$$

where for a Gaussian beam:

$$h(\omega, \sigma) = \exp\left[-\omega^2 \sigma^2 / c^2\right]. \quad (4.5)$$

For the dipole mode ($n = 1$) and $\varphi = 0$, using (3.9) and (4.4), it may be written:

$$\tilde{\kappa}_T(\sigma) = \frac{\kappa_T(\sigma)}{r_s} = \frac{1}{\pi a_m} \int_0^\infty d\omega \operatorname{Im}[\tilde{Z}_T^{(1)}(\omega)] h(\omega, \sigma) \quad (4.6)$$

where $\tilde{\kappa}_T(\sigma)$ is a loss factor per unit offset and usually it is called kick factor. For practical calculations often the long-range approximation is used [24]:

$$\tilde{\kappa}_T(\sigma) = \frac{c}{2\pi^2 a_m^3 \sigma_z^{1/2}} \sqrt{\frac{Z_0}{2\sigma}} \Gamma(1/4) \quad (4.7)$$

As it was shown in [25], the above expression (4.7) is a main term of the series expansion of the integral (4.4) in powers of the parameter ζ_0/σ_z with $\tilde{Z}_T^{(n)}$ expressed by formulae (4.1). For the PETRA III vacuum chamber of the standard straight section (see Table 1, No2) and a bunch length of $\sigma_z = 12$ mm the calculation for both cases gives the same result: $\kappa_T(\sigma) = 0.05431 \text{ V/pC m}^2$. Above formulae do not take into account the finite thickness of tube wall. For the tube with a finite wall thickness the formulae (3.2) should be used. For a single layer ($m = 1$) stainless steel tube with a wall thickness of 2 mm (see Tab. 2, No2) one obtains: $\kappa_T(\sigma) = 0.05439 \text{ V/pC m}^2$. The difference is less than 0.2%. For the same tube with NEG-coating (with a coating thickness of $1 \mu\text{m}$) the value of the kick factor is about 12% larger: $\kappa_T(\sigma) = 0.06073 \text{ V/pC m}^2$. In Fig. 9 the dependence of the kick factor on thickness of the wall is shown for the single layer tube and the NEG coated tube as well.

It follows from Fig. 9 that the kick factor for both cases is almost constant in a wide range down to a wall thickness of 0.01mm. In this region the kick factor practically coincides with the long-range approach and is independent from the wall thickness. In Fig. 10 the comparison of kick factor with the long-range approach is shown in more detail.

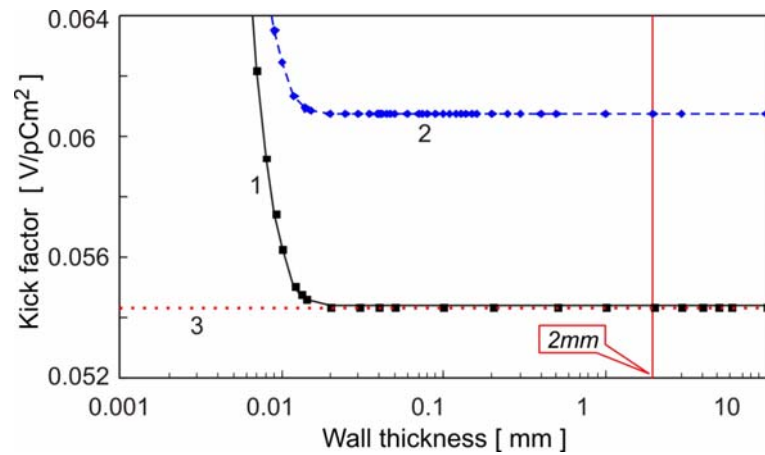


Fig.9: Kick factor versus tube wall thickness. Solid curve (1): single-layer stainless-steel tube with a radius of 47mm; dashed curve (2): the same tube with an inner NEG coating with a thickness of 1 μ m. The long-range approach is also shown (3).

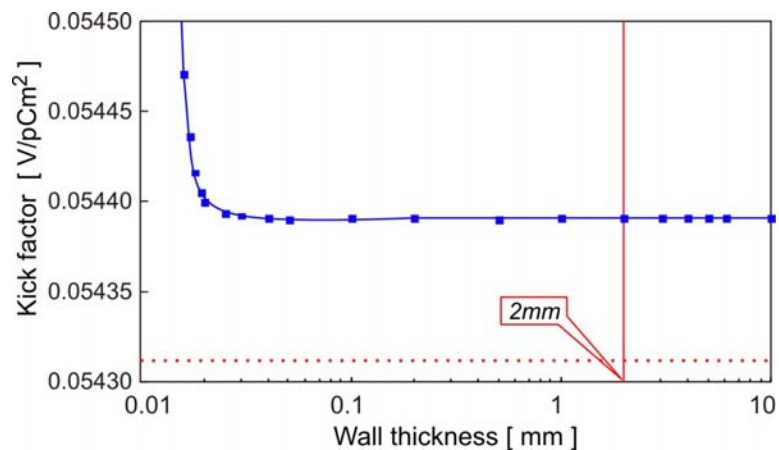


Fig.10: Single-layer tube kick factor versus wall thickness (solid curve) and long range approach (dotted).

The small difference between the long-range approximation and the exact curve is independent from the tube wall thickness and is caused by the low-frequency part of the impedance (see Fig. 5). The next figure (Fig.11) shows the small, damped oscillations of the kick factor, caused by the NEG coating. The kick factor for the thick wall is independent from the wall thickness and the value is close to that of a NEG-coated tube with an infinite wall.

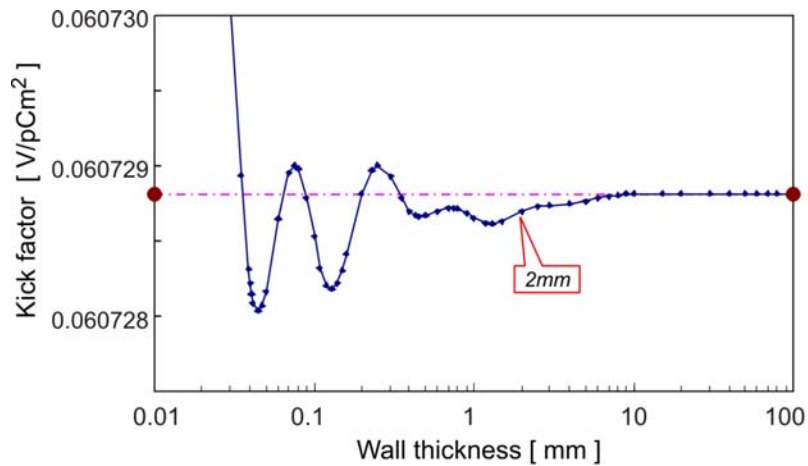


Fig.11: Kick factor of a NEG coated tube versus wall thickness.
The tube radius is 47mm and thickness of the coating is 1 μm .

Another limiting case is that of a very thin metallic wall. In Fig. 12 the kick factor of a NEG coated (thickness: 1 μm) stainless steel tube with a very thin wall is compared with the kick factor of a tube, which is completely made from NEG material with a wall thickness of 1 μm .

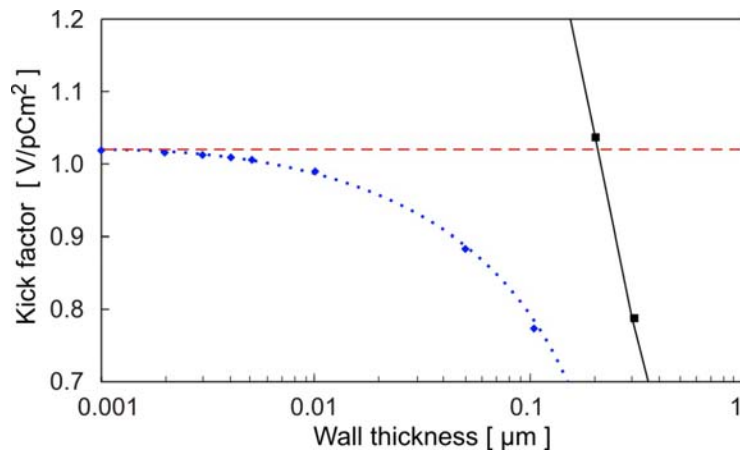


Fig.12: Kick factor of a NEG coated tube versus wall thickness for the case of very thin stainless steel wall; tube radius is 47mm, coat thickness is 1 μm (dotted curve). The dashed line is the kick factor for a tube with walls manufactured from NEG material with a thickness of 1 μm . The long-range approach of the kick factor (solid line) is also shown.

The other vacuum chambers from the list of Table 1 have elliptical cross sections (see No 1, 3 and 4 in Tab. 1). In the present report, these chambers are treated as circular chambers, using the smaller parameter of the ellipse as an equivalent circle diameter. In the Fig. 13, 14 and 15 the kick parameter is plotted versus tube thickness for the corresponding vacuum chamber cross sections (PETRA III standard arc, undulator and wiggler vacuum chambers). From the figures it follows, that

the exact value of the kick factor is without NEG coating close to the value calculated with the long-range approximation formula. Without NEG coating this is true for all four vacuum chambers from Tab. 1. If a vacuum chamber is coated with NEG material the difference may be significant, especially for a tube with a small inner radius (see Table 4).

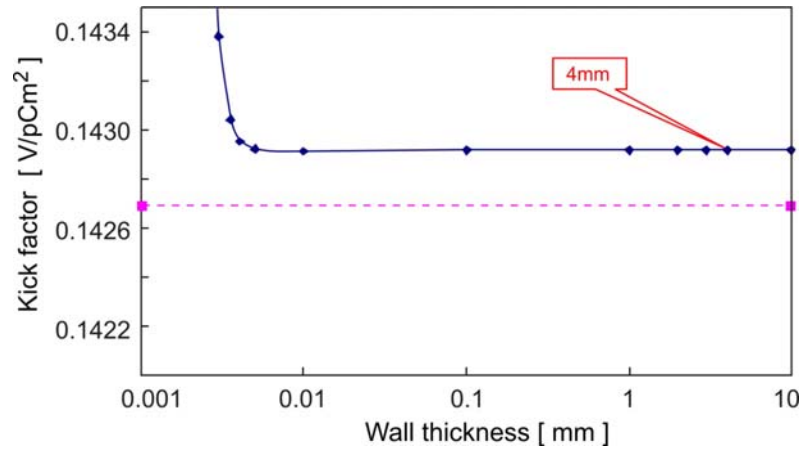


Fig. 13: PETRA III standard arc (Tab.1, No.1): kick factor versus wall thickness, calculated for a circular pipe without NEG coating and with an inner radius of 20 mm (solid); long-range approach (dashed).

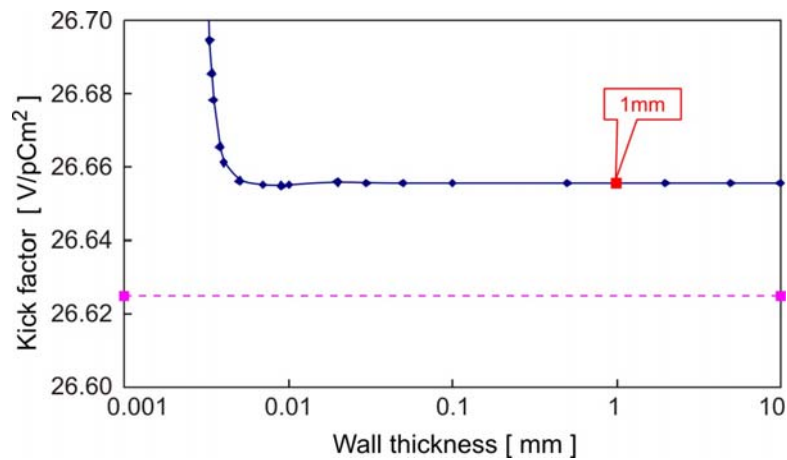


Fig. 14: Undulator vacuum chamber (Tab.1, No.3). Kick factor versus wall thickness, calculated for a circular pipe without NEG coating and with an inner radius 3.5 mm (solid); long-range approach (dashed)

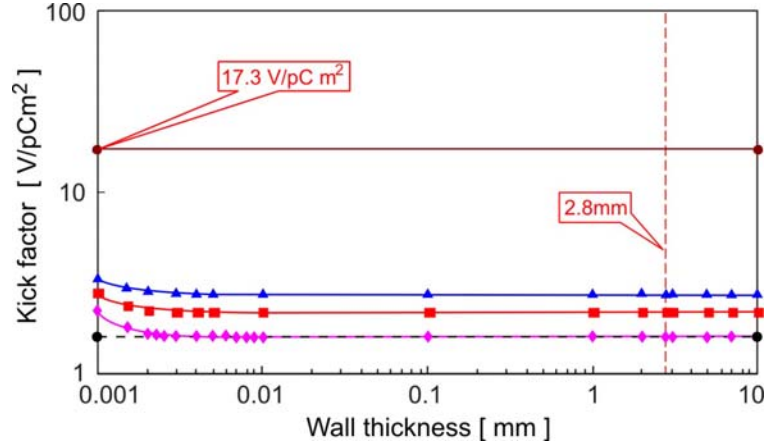


Fig. 15: Wiggler vacuum chamber (Tab.1, No.4). Kick factor versus wall thickness, calculated for a circular pipe with an inner radius of 8.95 mm: without NEG coating (diamond), and with NEG coating with a thickness of 0.5 μm (square) and 1 μm (triangle), long-range approach (dashed). The kick factor (17.3 V/pC m^2) for a tube, manufactured entirely of the NEG material, is also shown using the long-range approach (4.7).

N	Form		Inner dimensions	Wall thickness	k_T (V/pC m^2)			
					exact, without coating	exact, coating thickness 0.5 μm	exact, coating thickness 1 μm	Long-range approach
1	Elliptical	Al	$r_1=40\text{mm}$, $r_2=20\text{mm}$	4mm	0.142916	0.19532	0.24749	0.142693
2	Circular	SS	$R=47\text{mm}$	2mm	0.05439	0.05760	0.06073	0.05431
3	Elliptical	Al	$r_1=28.5\text{mm}$, $r_2=3.5\text{mm}$	1mm	26.6556	36.4348	46.1744	26.6249
4	Elliptical	Al	$r_1=48\text{mm}$, $r_2=8.95\text{mm}$	2.8mm	1.59461	2.17938	2.76163	1.59229

Table 4: Kick factors due to resistive walls for four different types of vacuum chambers. The vacuum chambers with elliptic cross sections have been approximated with round chambers.

4.6. Total kick parameter for resistive walls

The total kick parameter is calculated in the following way:

$$k_{\perp total} = \frac{1}{\langle \beta \rangle} \sum_i \beta_i k'_{i\perp} \quad (4.8)$$

where β_i is the beta function for the corresponding devices ($\beta_y = 5$ m for undulator section, $\beta_y = 15$ m for wiggler section and $\beta_y = 20$ m for the standard arc), $\langle\beta\rangle$ is the average beta function ($\langle\beta\rangle = 20$ m), $\kappa'_{\perp i} = \kappa_{\perp i} L_i$ (V / pC m), with L_i the length of corresponding device. Below, in Table 5 the parameters of PETRA III used for the total kick parameter calculation are given.

Device	Material	gap/mm	k_T (V/pC m ²)	Length (m)	k'_T (V/pC m)
Undulator	Al	7	26.6556	55	1466.06
Wiggler	Al+NEG	17.9	2.76163	80	220.93
Arc	Al	40	0.142916	1411	201.654

Table 5: Resistive wall kick factors for PETRA III devices.

Therefore, the total resistive wall kick parameter of the PETRA III devices is equal to

$$k_{\perp total} = \frac{1}{\langle\beta\rangle} \sum_i \beta_i k'_{i\perp} = 734 \text{ V/pC m} \quad (4.9)$$

4.7 Integral gradient of the longitudinal wake

The longitudinal wake field produces an additional gradient for the synchrotron oscillations. Since the field travels with the bunch it causes a bunch lengthening and a shift of the incoherent synchrotron frequency, but no change of the coherent synchrotron frequency [26]. A characteristic quantity for the longitudinal effects is the integral of the gradient of longitudinal wake potential, which is defined in the following way:

$$\kappa_{\parallel}(1) = \left| \frac{1}{\pi} \int_0^{\infty} d\omega k_c \text{Im}[Z_{\parallel}^{(0)}(\omega)] e^{-k_c^2 \sigma^2} \right|. \quad (4.10)$$

In Table 6 the parameter $\kappa_{\parallel}(1)$ due to the resistive wall is given in the cases of no NEG coating, and with NEG coating with a thickness 0.5 μm and 1 μm for the PETRA III vacuum chambers (Table 1, No 1-4).

N	Form		Inner dimensions	Wall thickness	$k_{ }(1) (V/pC m^2)$		
					exact, without coating	exact, coating thickness 0.5 μ m	exact, coating thickness 1 μ m
1	Elliptical	Al	$r_1=40\text{mm}, r_2=20\text{mm}$	4mm	0.049569	0.049727	0.050320
2	Circular	SS	$R=47\text{mm}$	2mm	0.104300	0.104525	0.105180
3	Elliptical	Al	$r_1=28.5\text{mm}, r_2=3.5\text{mm}$	1mm	0.283177	0.284060	0.287424
4	Elliptical	Al	$r_1=48\text{mm}, r_2=8.95\text{mm}$	2.8mm	0.110757	0.111104	0.1124226

Tab. 6: The longitudinal parameter $\kappa_{||}(1)$ for the PETRA III vacuum chambers (Table 1, No 1-4).

It is shown in Tab. 6, that the presence of the NEG coating is not significant for the calculated parameter $\kappa_{||}(1)$. In Table 7 a summary of parameters $\kappa_{||}(1)$ is presented for the PETRA III devices.

Device	Material	gap/mm	$k_{ }(1)(V/pC m^2)$	Length (m)	$k'_{ }(1)(V/pC m)$
Undulator	Al	7	0.283177	55	15.5747
Wiggler	Al+NEG	17.9	0.1124226	80	8.99381
Arc	Al	40	0.049569	1411	69.9419

Table 7: The parameters $\kappa_{||}(1)$ due to the resistive wall for the PETRA III vacuum chambers.

The total gradient of longitudinal wake is calculated as a sum over all vacuum chambers:

$$k(1)_{||total} = \sum_i k'(1)_{||i} = 94.5 V/pC m \quad (4.11)$$

As it can be seen from the previous numerical data (see Tabs 4-7), the NEG coating increases the kick and loss parameters. In the limit of a very thick coating the parameters tend to values for a pipe, which is composed totally from the NEG material (Fig. 16).

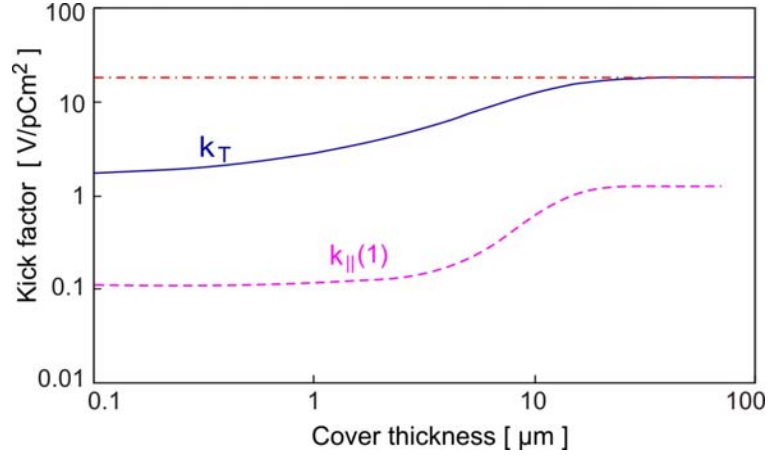


Fig.16: Kick factor (solid) and integral gradient of the longitudinal wake (dashed) versus cover thickness. The long-range approximation is plotted as well. The pipe radius is 8.95 mm, the wall material is aluminum, which is coated with NEG material.

4.8 PETRA III resistive impedance budget

The instability threshold for mode coupling instabilities can be estimated from the tune shifts of the lowest order modes in the longitudinal and transverse planes [27]:

$$\Delta Q_\beta = \frac{I_B \langle \beta \rangle T_0}{4\pi E/e} k_\perp, \quad \Delta Q_s = Q_s \frac{I_B R T_0}{2hV_{rf}} k_\parallel(1), \quad (4.12)$$

where I_B is the single bunch current, $R = 367m$ is the mean machine radius, and $\langle \beta \rangle$ is the average beta function. The following tolerable tune shifts are assumed [3]:

$$\frac{\Delta Q_\beta}{Q_s} = 0.5, \quad \frac{\Delta Q_s}{Q_s} = 0.5 \quad (4.13)$$

The maximal acceptable values for parameters k_\perp and $k_\parallel(1)$ can be obtained from the equations (4.12) and (4.13) [27]. Table 8 presents the total longitudinal and transverse impedance budget (in terms of k_\perp and $k_\parallel(1)$) for PETRA III (in the case of the single bunch current of 2.5mA) and resistive wall contribution to the budget.

PETRA III	$ k_\parallel(1) $ (V/pCm)	$ k_\perp $ (V/pCm)
Budget (total)	10900.00 (100%)	4800 (100%)
Resistive walls	94.5 (0.87%)	734 (15.3%)

Table 8: Total impedance budget and resistive wall impedance contribution to the budget for PETRA III.

The longitudinal and transverse resistive wall contributions to the total impedance budget are equal to 0.87% and 15.3% respectively.

5. Conclusion

In the present Report the results of theoretical and numerical investigations have been presented. The new results, given in the Chapter 3, may be considered as a final solution for the multilayer round tube impedance problem. The exact formulae are obtained for the point-like charge coupling impedance for the case of arbitrary γ . The formulae are compact and are convenient both for theoretical investigations and numerical calculations. The contribution of the resistive wall impedance in terms of the kick factor and the integrated gradient of the longitudinal wake potential to the total impedance budget has been estimated. The goal of future investigations will be to obtain an improved solution for the impedances of multilayer vacuum chamber with elliptical cross section and its application to the PETRA III vacuum chambers with elliptical cross section.

6. Acknowledgment

The authors would like to express thanks to Klaus Balewski, Winfried Decking and Vitali Khachatryan for stimulating discussions. This work was partly supported by CRDF Grant ARP2-3233-YE-04.

7. References

1. private communications:
DESY vacuum group: Vacuum Chamber Cross Sections,
S. Calatroni, CERN: resistivity of TiVCr films.
2. "PETRA III: A low Emittance Synchrotron Radiation Source", Technical Design Report, DESY 2004-035; http://petra3.desy.de/project_description
3. A.W. Chao, Physics of Collective Beam Instabilities in High Energy Accelerators (Wiley, New York, 1993).
4. K.L.F. Bane and M. Sands, SLAC-PUB-95-7074, December 1995.
5. B.W.Zotter and S. A. Kheifetz, Impedances and Wakes in High-Energy Particle Accelerators, World Scientific, Singapore, 1997.
6. B. Zotter, Part. Accel. 1, 311 (1970).
7. B. Zotter, CERN Technical Report No. 69-15, 1969.

8. A.Burov and V.Lebedev, FERMILAB-Conf-02/100-T, June 2002.
9. A.M. Al-khateeb, O. Boine-Frankenheim, R. W. Hasse, and I. Hofmann, Phys. Rev. E, 71, 026501 (2005).
10. J.D Jackson, SSC-N-110, Jan 1986.
11. D. Briggs, SSCL-512-REV1, Jun 1992.
12. E. Keil and B. Zotter, EPAC'98, Stockholm, pp. 963-965, 1998.
13. A. Piwinski, IEEE Trans.Nucl.Sci. 24, No.3, pp. 1364-1366, 1977.
14. G.R. Lambertson, LBL-44454, LBNL-44454, Aug 1999.
15. A. Burov and A. Novokhatski, Preprint 90-28, INP-Novosibirsk, 1990.
16. R. Nagaoka, EPAC 2004, pp. 2038-2040.
17. F. Ruggiero, Part. Accel. 50: pp. 83-104, 1995.
18. M. Ivanyan and V. Tsakanov, Phys. Rev. ST Accel. Beams, 7, 114402 (2004).
19. M. Ivanyan and A. Tsakanian, Phys. Rev. ST Accel. Beams, 9, 034404 (2006).
20. T. Perron, L.Farvacque, and E.Plouviez, EPAC 2004, pp. 2053-2055
21. T.F. Gunzel, Phys. Rev. ST Accel. Beams, 9, 114402 (2006).
22. T. Weiland and R. Wanzenberg, 1990 Joint US-CERN Accelerator Courses, Hilton Head, So Carolina, DESY M 91-06, May 1991.
23. A. Piwinski, Report No. DESY HERA 92-11, 1992, p. 19.
24. O. Henry and O. Napoly, Part. Acc. Vol. 25, pp.235-247, 1991.
25. M. Ivanian and V. Tsakanov, DESY-TESLA-2003-25, Oct 2003. 11pp. Published in Nucl.Instrum.Meth.A522: 223-229, 2004.
26. A. Piwinski, Report No DESY 84-097, Oct 1984.
27. K. Balewski and R. Wanzenberg, Proceedings of 2005 Particle Accelerator Conference, Knoxville, Tennessee, USA, pp. 1751-1753, 2005.